

CEACAM1 regulates insulin clearance in liver

Matthew N. Poy¹, Yan Yang¹, Khadijeh Rezaei¹, Mats A. Fernström¹, Abraham D. Lee², Yoshiaki Kido³, Sandra K. Erickson⁴ & Sonia M. Najjar¹

Published online: 19 February 2002, DOI: 10.1038/ng840

We hypothesized that insulin stimulates phosphorylation of CEACAM1 which in turn leads to upregulation of receptor-mediated insulin endocytosis and degradation in the hepatocyte. We have generated transgenic mice over-expressing in liver a dominant-negative, phosphorylation-defective S503A-CEACAM1 mutant. Supporting our hypothesis, we found that S503A-CEACAM1 transgenic mice developed hyperinsulinemia resulting from impaired insulin clearance. The hyperinsulinemia caused secondary insulin resistance with impaired glucose tolerance and random, but not fasting, hyperglycemia. Transgenic mice developed visceral adiposity with increased amounts of plasma free fatty acids and plasma and hepatic triglycerides. These findings suggest a mechanism through which insulin signaling regulates insulin sensitivity by modulating hepatic insulin clearance.

Introduction

Insulin activates different intracellular signaling pathways by promoting protein phosphorylation. The insulin receptor is a ligand-activated tyrosine kinase that activates many intracellular protein substrates. Insulin-receptor substrates (IRSs) have been shown to influence insulin signaling in different tissues by promoting the activation of phosphatidylinositol-3 (PI-3) kinase and a set of PIP-dependent serine/threonine protein kinases¹. It is likely, however, that additional substrates are also required for insulin action. For example, a pathway mediated by phosphorylation of the proto-oncogene c-cbl can lead to glucose uptake independent of PI-3 kinase in response to insulin². Similarly, α_2 -Heremans Schmid glycoprotein (α_2 -HSG) inhibits signaling through the insulin receptor kinase³, as can the plasma cell membrane glycoprotein-1 (PC-1)⁴.

We showed previously that the transmembrane glycoprotein CEACAM1 is phosphorylated in response to insulin in hepatocytes⁵. The insulin receptor kinase phosphorylates a single tyrosine residue (Tyr488) in the intracellular domain of CEACAM1. In addition, CEACAM1 is phosphorylated by serine/threonine kinases on Ser503 in the absence of insulin. Substituting Ala for Ser503 effectively abolished CEACAM1 phosphorylation by either serine/threonine or tyrosine kinases, suggesting that phosphorylation on Ser503 is required for subsequent tyrosine phosphorylation by the insulin receptor kinase.

The function of CEACAM1 remains elusive. It has been proposed to act as a cell adhesion molecule⁶. It is also known to suppress tumor growth in cells of epithelial origin^{7–10}, to downregulate the mitogenic effects of insulin and to upregulate receptor-mediated insulin endocytosis and degradation^{11–13}. Phosphorylation of CEACAM1 seems to be required for its effect on cell proliferation and insulin degradation^{12,13}. *In vitro* studies

suggest that upon its phosphorylation by the insulin receptor kinase, CEACAM1 binds indirectly to the receptor to undergo internalization in clathrin-coated vesicles¹⁴ as part of the insulin endocytosis complex. Because receptor-mediated insulin endocytosis and degradation in the hepatocyte constitutes the principal mechanism of insulin clearance, which occurs mostly in liver¹⁵, we have proposed that CEACAM1 phosphorylation modulates hepatic insulin clearance, contributing to the regulation of systemic insulin concentrations.

Because of the presence of two closely related *Ceacam* genes in mouse (as opposed to one gene in rat and humans)¹⁶, we generated a mouse model of functional inactivation of *Ceacam1* bearing a dominant-negative, phosphorylation-defective CEACAM1 mutant (from S503A rat) in liver. We report that over-expression of the S503A minigene restricted to liver results in hyperinsulinemia due to impaired insulin clearance, with secondary hepatic insulin resistance and impaired glucose tolerance in the liver-specific S503A CEACAM1 mutant (L-SACC1) mice. These data indicate a new mechanistic link between insulin signaling and regulation of peripheral insulin sensitivity.

Results

Phosphorylation of CEACAM1 in L-SACC1 mice

We characterized and bred to homozygosity a mouse line (F0 113) carrying six copies of the rat *Ceacam1* S503A transgene. After phosphorylating liver lysates in the presence of [γ -³²P]ATP, we immunoprecipitated proteins with specific antibodies against rat CEACAM1 (α -rCC1; Fig. 2b) and mouse BGP, the rat CEACAM1 homolog (Fig. 2a). In contrast to the wild type (Fig. 2a, lanes 3 and 4), insulin failed to stimulate CEACAM1 phosphorylation in homozygous L-SACC1 (L-SACC1^{homo}) mice (Fig. 2a, lanes 1 and 2). Overexpressing this mutant did not significantly

¹Departments of Pharmacology and Therapeutics, and ²Physical Therapy, Medical College of Ohio, 3035 Arlington Avenue, HSci Building Room 270, Toledo, Ohio 43614, USA. ³Second Department of Internal Medicine, Kobe University School of Medicine, 7-5-1 Kusunoki-cho, Chuo-ku, Kobe, Japan. ⁴Department of Medicine, San Francisco and the Veterans Affairs Medical Center, University of California, San Francisco, California, USA. Correspondence should be addressed to S.M.N. (e-mail: snajjar@mco.edu).



decrease phosphorylation of either the insulin receptor (Fig. 2d, lanes 1 and 2) or IRS-2 (Fig. 2e, lanes 1 and 2), a major substrate of the insulin receptor kinase in liver. These results indicate that abolishing CEACAM1 phosphorylation in liver does not interfere with phosphorylation of other substrates of the insulin receptor. It is thus possible that IRS-dependent signaling pathways and the insulin actions they mediate are not altered in L-SACC1 mice.

The S503A transgene causes hyperinsulinemia

L-SACC1^{homo} mice showed increased body weight (Fig. 3a; $P < 0.05$) and visceral adiposity at all ages examined ($P < 0.05$; Fig. 3b). By contrast, hemizygous (L-SACC1^{hemi}) mice were not different from wildtype mice, consistent with a gene-dosage effect (Fig. 3a). Liver, kidney and muscle functions were unaltered (Table 1). L-SACC1^{homo} mice at two and eight months showed a 200–500% increase in plasma insulin levels compared with age-matched wildtype mice (Fig. 4a[i]). Insulin clearance, measured as fasting molar C-peptide/insulin ratio, was significantly reduced in L-SACC1^{homo} mice (Fig. 4a[iii]). Moreover, the amount of plasma residual

[¹²⁵I]-insulin at 60–90 min after tail injection was 200–300% higher in L-SACC1 than wildtype animals (Fig. 4b). Insulin internalization was decreased by approximately 50% ($P < 0.05$) in hepatocytes of L-SACC1^{homo} mice (Fig. 4c). In addition, insulin-induced internalization of insulin receptors and CEACAM1, as measured by the loss of biotin-labeled surface membrane proteins¹⁴, was reduced in L-SACC1 compared with wildtype animals (insulin receptor: 49.4% in L-SACC1 versus 82.1% in wildtype; CEACAM1: 13.7% in L-SACC1 versus 41.3 in wildtype; Fig. 4d). Because CEACAM1 undergoes internalization with the insulin receptor as part of the insulin endocytosis complex¹⁴, these findings indicate that receptor-mediated insulin internalization and degradation were decreased in L-SACC1 mice. That C-peptide levels in L-SACC1^{homo} mice were mildly increased (Fig. 4a[ii]; $P < 0.05$) was further supported by unaltered β -cell mass (1.611 ± 0.742 in L-SACC1 versus 1.717 ± 0.75 in wildtype, $P > 0.05$). Taken together, these findings suggest that the primary abnormality of insulin metabolism in L-SACC1 mice is impaired insulin clearance rather than increased insulin secretion.

To address whether hyperinsulinemia was a primary effect of the transgene or secondary to insulin resistance, we examined insulin sensitivity by intraperitoneal insulin tolerance. After insulin injection, glucose levels decreased to a similar extent in L-SACC1^{homo} and controls (wildtype and L-SACC1^{hemi} mice) at two and eight months of age (Fig. 4e). This suggests that peripheral tissues maintained insulin sensitivity in L-SACC1^{homo} mice. In control mice, glucose levels returned to normal within three hours, whereas in L-SACC1^{homo} they remained suppressed. These results support the possibility that injected insulin was cleared less efficiently.

Secondary insulin resistance in L-SACC1 mice

L-SACC1^{homo} mice developed mild random hyperglycemia at 2–8 months (Fig. 5a), indicating insulin resistance in these mice. Fasting glucose levels were unaltered, however, at two months (Fig. 5b; 113 ± 37 in L-SACC1^{homo} versus 133 ± 41 in wildtype, $P > 0.05$) or ten months (Fig. 5b; 143 ± 19 in L-SACC1^{homo} versus 124 ± 29 in wildtype, $P > 0.05$). Moreover, L-SACC1^{homo} mice were glucose intolerant (Fig. 5b). The discrepancy between their sensitivity to insulin in an insulin tolerance test and their glucose intolerance probably has several causes. First, the large doses of insulin used in the insulin tolerance test are sufficient to overcome the mild degree of peripheral insulin resistance. Second, the degree of hypoglycemia occurring during an insulin tolerance test depends largely on insulin-dependent glucose uptake that occurs primarily in skeletal muscle, whereas hyperglycemia following an intraperitoneal glucose injection in rodents disproportionately depends on glucose utilization in liver. Thus, the prediction from these experiments would be that L-SACC1 has secondary hepatic with

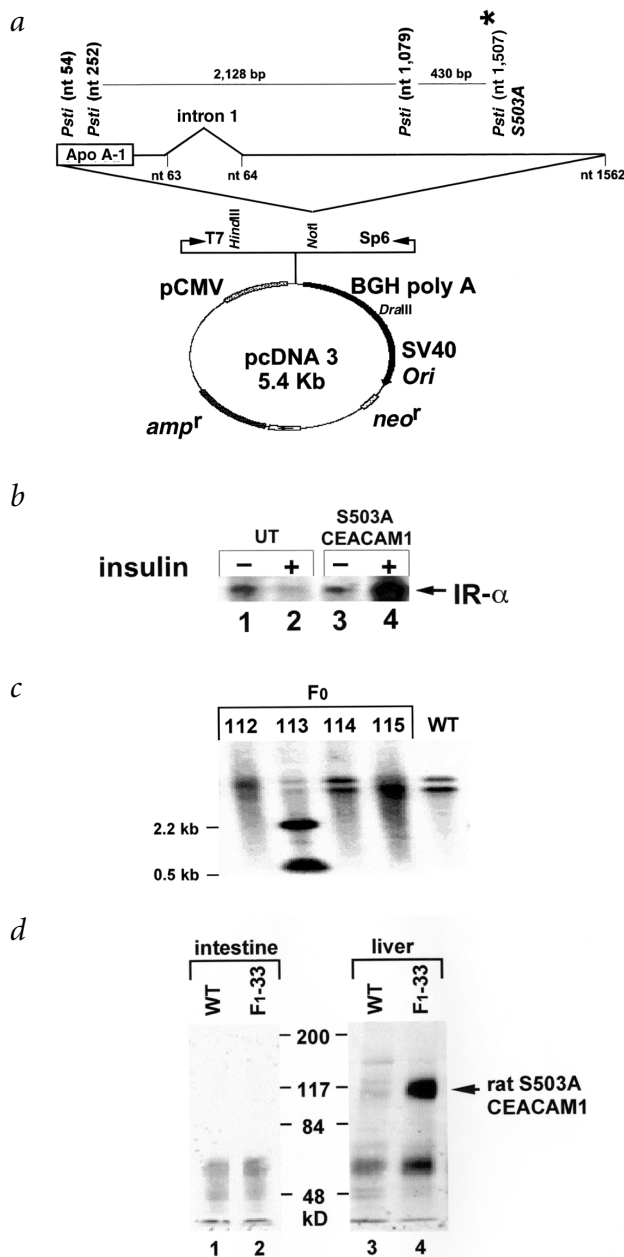


Fig. 1 Generation of L-SACC1 mice. **a**, Subcloning of Apo A-1 promoter upstream of a Ceacam1 rat minigene bearing a Ser → Ala mutation on aa 503. The mutation created a new *Pst*I site (*) without changing the reading frame of the rat mutant protein. **b**, Dominant-negative effect of rat S503A CEACAM1. SV40-transformed mouse hepatocytes were transfected with rat S503A CEACAM1 mutant (lanes 3, 4) or left untransfected (UT; lanes 1, 2). Internalization of the insulin receptor was measured as the loss of biotin-labeled α -subunit of the insulin receptor (IR- α) from the surface in the presence (even lanes) versus absence (odd lanes) of insulin. **c**, Southern blot of *Hind*III/*Pst*I-digested genomic DNA from animal tails, using a [³²P]-labeled Apo A-1 promoter/S503A Ceacam1 minigene as a probe. In the representative gel, bands derived from the transgene were detected in the F0 mouse 113 in addition to the bands derived from the endogenous gene that is also detected in wildtype (WT) animals. **d**, Western blot of liver-specific expression of S503A CEACAM1 proteins. Plasma membrane proteins from livers and small intestines of F1 progeny and WT mice were prepared by detergent extraction and partial purification on lectin chromatography. Equal amounts (300 mg) of glycoproteins were immunoprecipitated with R2-6, a polyclonal rat CEACAM1 antibody that cross-reacts with the mouse protein. After analysis on 7% SDS-PAGE, proteins were immunoblotted with α -295, a polyclonal rat CEACAM1 antibody, and detected by ECL.



insignificant muscle insulin resistance. In fact, insulin induced a comparable rise in the rate of glucose uptake in soleus muscle of 2-month wild-type and L-SACC1 mice at submaximal concentrations (1.2 nM ; 5.20 ± 0.98 in wildtype versus $3.73 \pm 0.54 \text{ nmol g}^{-1} \text{ min}^{-1}$ in L-SACC1, $P < 0.05$; Fig. 5c). Similar results were obtained in epitrochlearis muscles of mice at two and six months (data not shown). In addition, glucose transporter-4 (GLUT4) mRNA levels were not altered in soleus muscle of L-SACC1 mice (Fig. 5d). Moreover, the triglyceride content in soleus muscle of 8-month L-SACC1 mice was normal (66 ± 16 in L-SACC1 mice versus $45 \pm 9 \text{ mg mg}^{-1}$ protein in wild-type, $P > 0.05$). These findings indicate that L-SACC1 mice do not develop significant muscle insulin resistance.

The receptor number in hepatocytes was reduced by half in L-SACC1^{homo} mice at two and eight months (approximately $2.4 \pm 0.28 \times 10^4$ in L-SACC1 versus approximately $5.62 \pm 0.85 \times 10^4$ receptors per cell in wildtype, $P < 0.05$). Moreover, the affinity of insulin binding (K_d) was virtually unchanged ($4.97 \pm 0.55 \times 10^{-8}$ in L-SACC1 versus $6.55 \pm 1.20 \times 10^{-8}$ in wildtype, $P > 0.05$). Steady-state mRNA encoding a rate-control enzyme for hepatic gluconeogenesis, phosphoenolpyruvate carboxykinase (PEPCK), was consistently significantly higher (by approximately 150–600%) in homozygous L-SACC1 at all ages examined (Fig. 5e). This suggests that primary hyperinsulinemia caused secondary hepatic insulin resistance in L-SACC1 mice. In contrast, mRNA encoding a rate-control enzyme in glycogenolysis, glycogen 6-phosphatase (G-6-Pase), was 35–70% lower in L-SACC1^{homo} than in wildtype mice (Fig. 5e). The decrease in G-6-Pase could counter-regulate the positive effect of elevated PEPCK on hepatic glucose production. This is consistent with a condition of hepatic insulin resistance secondary to hyperinsulinemia without a significant increase in fasting glucose levels and development of diabetes in L-SACC1 mice.

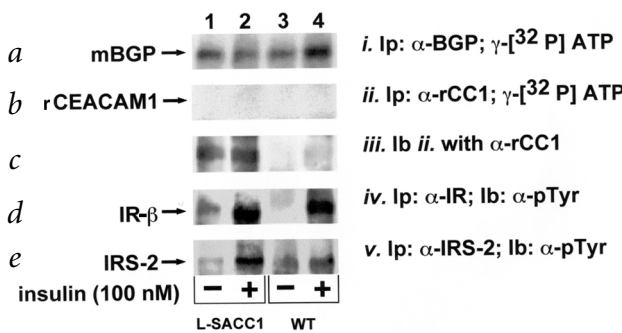


Fig. 2 Specific alteration of hepatic CEACAM1 phosphorylation in L-SACC1 mice. **a–e**, Glycoproteins from liver lysates of wildtype and L-SACC1 homozygous mice at 2 mo were lectin-purified and phosphorylated in the presence (**a–c**) or absence (**d,e**) of [$\gamma^{32}\text{P}$]ATP. Proteins were then immunoprecipitated (Ip) with antibodies against mouse biliary glycoprotein ($\alpha\text{-mBGP}$), the mouse CEACAM1 homolog; **a**; rat CEACAM1 ($\alpha\text{-rCC1}$); **b**; IR- β subunit (IR- β ; **d**) and IRS-2 (**e**). Phosphorylation of proteins was detected by autoradiography (**a–b**) and immunoblotting (**lb**) with α -phosphotyrosine antibody ($\alpha\text{-pTyr}$; **d–e**). To account for the amount of rat CEACAM1 in the immunopellets, blot **b** was reprobed with $\alpha\text{-rCC1}$ (**c**).

Table 1 • Biochemistry of normal liver, kidney and muscle in homozygous L-SACC1 mice

	WT	L-SACC1 ^{homo}
Liver function		
Aspartate aminotransferase (μM)	127.8 ± 35.8	123.5 ± 52.3
Alanine aminotransferase (μM)	48.7 ± 15.1	63.6 ± 20.9
Alkaline phosphatase (μM)	48.0 ± 12.8	60.9 ± 21.5
Bilirubin: total (mg/dL)	0.18 ± 0.04	0.19 ± 0.09
Bilirubin: direct (mg/dL)	0.09 ± 0.03	0.10 ± 0.05
Cholesterol: total (mg/dL)	98.5 ± 9.74	97.5 ± 9.83
Cholesterol: HDL (mg/dL)	83.2 ± 3.80	92.6 ± 7.20
Muscle function:		
Creatine kinase (μM)	364.4 ± 141.8	337.5 ± 144.2
Kidney function:		
Blood urea nitrogen (mg/dL)	27.5 ± 2.80	35.0 ± 3.90

The levels of several enzymes and of cholesterol, bilirubin and blood urea nitrogen were determined in fasting wildtype (WT) and homozygous (homo) L-SACC1 mice at 8 mo. All assays were carried out in triplicate. Values are expressed as mean \pm s.e.m.. $P > 0.05$ versus WT mice in all determinations.

Unaltered pancreatic β -cell function in L-SACC1 mice

To examine pancreatic β -cell function, we measured insulin secretion in response to glucose. Calculation of the area under the curve (Fig. 6) revealed that the first-phase insulin response to glucose was not altered ($P > 0.05$) in 10-month L-SACC1^{homo} mice (4.680 ± 2.157 a.u.) compared with controls (wildtype: 4.608 ± 1.142 and L-SACC1^{hemi}: 3.478 ± 0.728 a.u.). Similar results were obtained in mice at two months (data not shown). This suggests that hyperinsulinemia and hepatic insulin resistance did not significantly impair β -cell function in L-SACC1^{homo} mice, in agreement with no development of diabetes in these mice.

Altered fat metabolism in L-SACC1 mice

Because elevated FFA levels influence hepatic autoregulation of glucose production, perhaps by stimulating gluconeogenesis and downregulating glycogenolysis in mice¹⁷, we examined fasting plasma FFA levels in L-SACC1^{homo} mice. Plasma FFA were significantly elevated in these mice (Table 2; $P < 0.05$). This was associated with increased plasma (Table 2) and hepatic triglyceride content (18 ± 1 in L-SACC1 mice versus $10 \pm 3 \text{ mg mg}^{-1}$ protein in wildtype, $P < 0.05$).

Discussion

We have demonstrated that over-expression of a phosphorylation-defective *Ceacam1* transgene in mouse liver acts in a dominant-negative manner to inhibit CEACAM1 function and results in hyperinsulinemia without altering liver function or insulin-signaling through other pathways. This is in marked contrast to mice bearing a liver-specific ablation of the insulin-receptor gene (LIRKO) that have altered liver function and IRS-dependent signaling pathways¹⁸. Hyperinsulinemia in L-SACC1 mice is consistent with the hypothesis that CEACAM1 is part of a complex of proteins required for internalization of the insulin-receptor complex^{11,12,14,19}. That hyperinsulinemia in L-SACC1 mice is primarily due to decreased hepatic clearance is supported by several findings: (i) the increase in insulin levels is not paralleled by a proportional increase in C-peptide levels (ii) β -cell mass is not commensurate to the extent of hyperinsulinemia (iii) L-SACC1 mice are more sensitive to exogenously administered insulin than nontransgenic littermates and (iv) L-SACC1 mice developed intra-abdominal visceral adiposity and elevated plasma FFA, which are commonly associated with impaired insulin clearance^{20–25}.

Other findings support the hypothesis that random hyperglycemia and impaired glucose tolerance in L-SACC1 mice are probably due to hepatic insulin resistance: (i) decreased numbers and internalization of insulin receptors with decreased internalization of insulin and CEACAM1 in primary hepatocytes derived

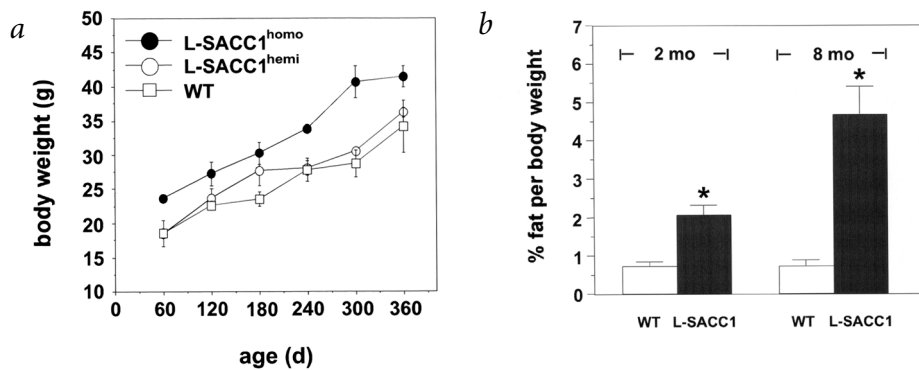


Fig. 3 Growth curves of age-matched wildtype and L-SACC1 mice. **a**, Wildtype (WT), L-SACC1^{homo} and L-SACC1^{hemi} mice were weighed at 2–12 mo. Values are expressed as mean \pm s.d. from six litters and represent 20 mice per genotype. $P < 0.05$ for L-SACC1^{homo} versus WT, and $P > 0.05$ for L-SACC1^{hemi} versus WT. **b**, Visceral adipose tissues from the abdominal region were collected from at least 15 L-SACC1^{homo} and WT mice and weighed and measured as a percentage of total body weight. Values are expressed as mean \pm s.d.; $P < 0.05$ for L-SACC1 versus WT.

from L-SACC1 mice (ii) elevated PEPCK mRNA levels (iii) normal insulin-dependent glucose uptake in isolated muscle, suggesting that hyperglycemia in L-SACC1 mice is due to increased hepatic glucose production rather than impaired muscle glucose uptake and (iv) elevated plasma FFA in L-SACC1 mice. This would contribute to hepatic insulin resistance by stimulating hepatic synthesis and output of glucose²⁶ and triglycerides²⁷. The phenotype of L-SACC1 mice is consistent with the secondary hepatic insulin resistance observed in recipients of pancreas transplants, in whom systemic delivery of insulin is associated with hyperinsulinemia and decreased first-pass insulin clearance

in liver^{28,29}. Although hyperinsulinemia in L-SACC1 mice is similar to that of LIRKO mice, the mechanism of its development differs in these two models. In L-SACC1 mice, hyperinsulinemia resulted mainly from impaired insulin clearance and, in turn, caused secondary hepatic insulin resistance, whereas in the LIRKO mouse, primary hepatic insulin resistance caused impaired insulin clearance, insulin hypersecretion and extreme hyperinsulinemia¹⁸. Nevertheless, neither mouse model of hepatic insulin resistance developed diabetes, supporting the notion that additional tissues must be involved for the development of overt type 2 diabetes.

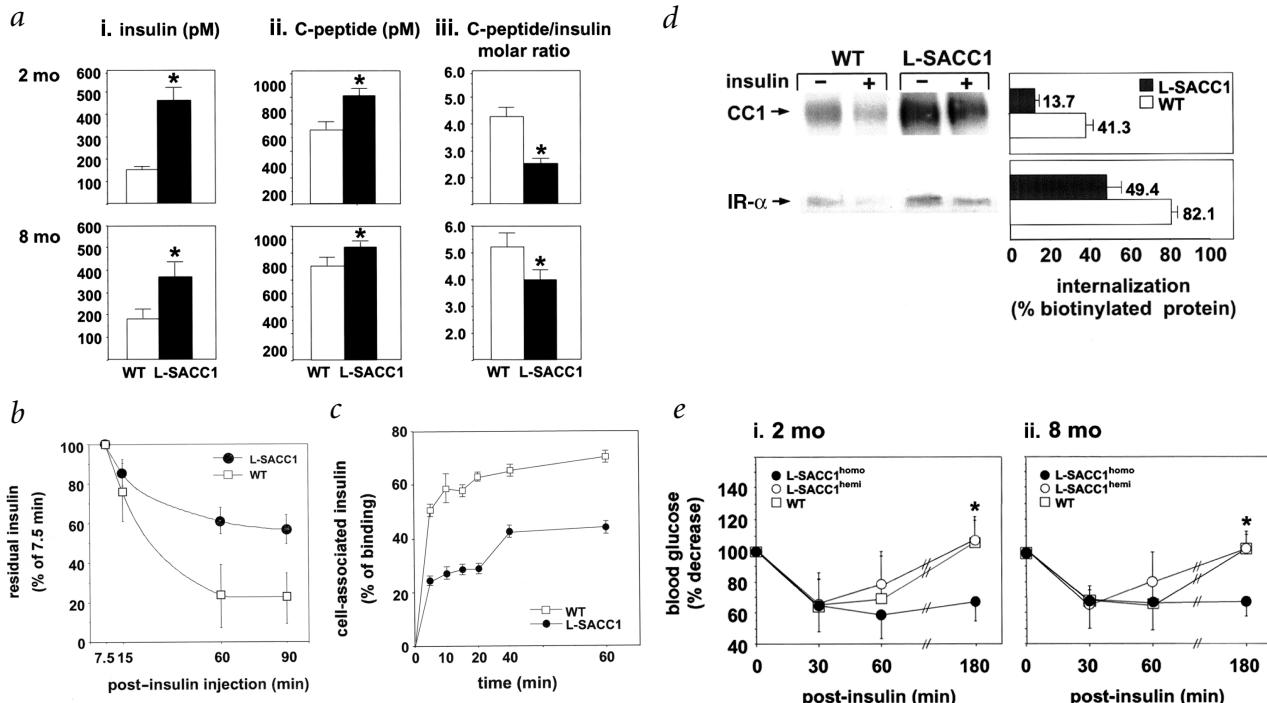
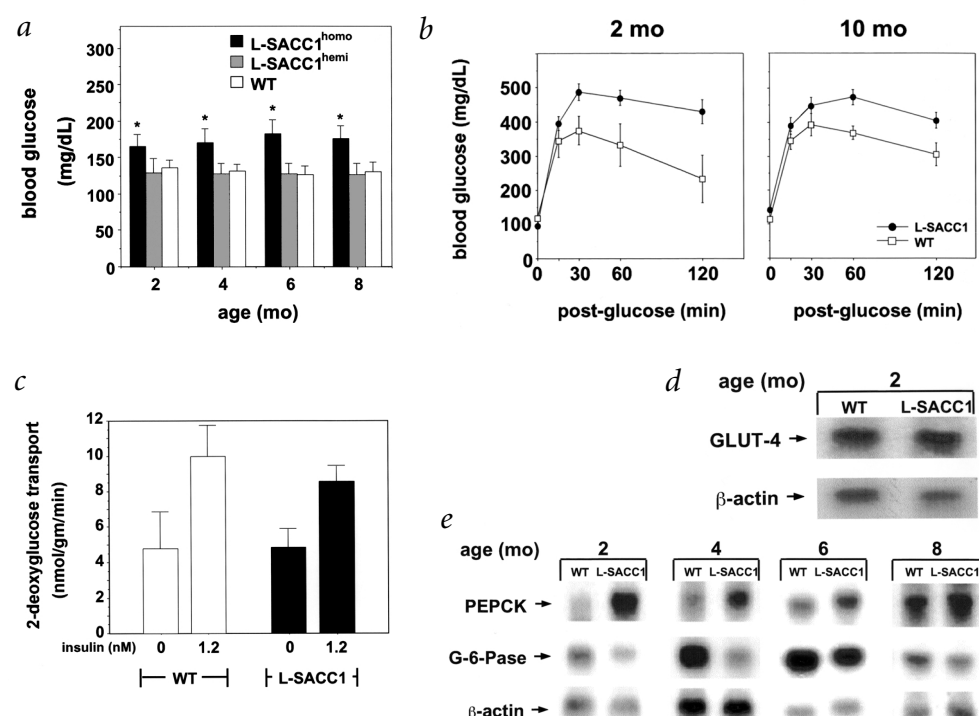


Fig. 4 Hyperinsulinemia in L-SACC1 mice is due to impaired insulin clearance. **a**, Plasma insulin (i) and C-peptide (ii) levels were measured in whole venous blood drawn between 11:00 am and 1:00 pm from 2-mo and 8-mo age-matched wildtype (WT) and L-SACC1^{homo} mice fasted overnight. Insulin clearance was calculated as the molar ratio of C-peptide to insulin (iii). Data represent at least three sets of experiments with at least 30 mice of each genotype. Values are expressed as mean \pm s.d.. Asterisks indicate a statistically significant difference ($P < 0.05$ by one factor ANOVA). **b**, Metabolic clearance of [¹²⁵I]-insulin injected in tail vein was measured in 8-mo WT (open squares) and L-SACC1^{homo} mice (closed circles). Values are expressed as mean \pm s.e.m. of the percent of the amount of plasma insulin at 7.5 min from eight mice of each genotype. **c**, [¹²⁵I]-insulin internalization in primary hepatocytes derived from age-matched WT (open squares) and L-SACC1 mice (closed circles) was measured. After binding, [¹²⁵I]-insulin was allowed to internalize at 37 °C for 0–90 min, as indicated on the horizontal axis. Internalized ligand was plotted on the vertical axis as percent of specifically bound ligand. Values are expressed as mean \pm s.d. from triplicate experiments carried out on at least three age-matched mice of each genotype. **d**, Primary hepatocytes derived from WT and L-SACC1^{homo} mice were treated with buffer (−, lanes) or insulin (+, lanes) before the labeling of cell-surface proteins with biotin. Cells were lysed and the proteins immunoprecipitated with polyclonal antibodies against mouse CEACAM1 (CC1) and the α -subunit of the insulin receptor (IR- α) prior to analysis by 7% SDS-PAGE, immunoblotting with HRP-labeled streptavidin and detection by ECL. The amount of CC1 and IR- α internalized in response to insulin was calculated as the difference in the amount of biotin-labeled proteins before and after insulin treatment relative to the amount of biotin-labeled proteins in the absence of insulin (graph). Experiments were repeated on at least three mice for each genotype. **e**, Insulin tolerance test. Glucose levels were measured in venous blood from age-matched wildtype (WT, open squares), L-SACC1^{hemi} (open circles) and L-SACC1^{homo} (closed circles) L- mice injected i.p. with insulin (0.125 U kg⁻¹) and fasted overnight. Data represent the mean \pm s.d. of 24 mice from each genotype. *Statistically significant difference ($P < 0.05$), WT versus L-SACC1^{hemi}.

Fig. 5 Secondary insulin resistance in L-SACC1 mice. *a*, Random glucose levels were measured in venous blood drawn at 10:00 am from 15 anesthetized age-matched mice. Data are the mean of two determinations per mouse carried out seven days apart at the same time period. Values are expressed as mean \pm s.d. Asterisks denote statistically significant difference ($P < 0.05$) between L-SACC1^{homo} mice and controls (WT and L-SACC1^{hemi}). *b*, Glucose tolerance test. Whole-blood glucose was determined at 0–120 min after glucose injection (2 mg kg⁻¹) of age-matched 2 mo and 10 mo WT and L-SACC1^{homo} mice fasted overnight. Values are expressed as mean \pm s.d. for at least 12 mice in each group. *c*, Insulin-dependent 2-deoxy-D-glucose (2-DG) uptake was measured in insulin-treated (1.2 nM) isolated soleus muscles from age-matched 2-mo mice that had been fasted. Values are expressed as mean \pm s.d. of eight samples for each mouse genotype. *d,e*, Poly (A)⁺ mRNA was purified from soleus muscle (*d*) and from livers (*e*) of age-matched WT and L-SACC1^{homo} mice at 2–8 mo. Results are representative of at least four mice from each genotype at each age.



Hyperinsulinemia in L-SACC1 mice did not parallel the extent of the metabolic alteration with hyperglycemia, suggesting that additional mechanisms underlie insulin resistance. The association of hepatic insulin resistance with elevation in FFAs and increased visceral adiposity provides a potential mechanism to explain this apparent discrepancy. Our model supports the hypothesis that decreased insulin clearance in the presence of increased abdominal adiposity and circulating FFA provides an alternative compensatory mechanism of peripheral insulin resistance^{30,31}.

Hypertriglyceridemia in L-SACC1 mice may at least partially be attributed to hyperinsulinemia³² and to increased glucose-induced *de novo* hepatic fatty-acid synthesis and lipogenesis. The increase in plasma triglycerides may, in turn, promote elevation in plasma FFA. For instance, it is possible that not all unesterified fatty acids released from hydrolysis of triglycerides by lipoprotein lipase are transported into adipocytes; some may remain albumin-borne in the blood. Based on the Randle cycle^{33,34}, it is reasonable to predict that chronic stimulation of glucose uptake in muscle by chronically elevated insulin levels would compete with FFA uptake in muscle and decrease FFA oxidation and clearance. We therefore hypothesize that elevation in plasma FFA in our model results from increased trigly-

ceride release from liver rather than from increased lipolysis in adipocytes. This is in agreement with observations of unaltered lipolysis with attendant decreased FFA reesterification in the peripheral tissues of obese subjects with higher insulin concentrations than their lean controls³⁵. Alternatively, elevated plasma FFA could result from increased *de novo* tissue lipogenesis in proportion to increased insulin levels in L-SACC1 mice, as has been reported in hyperinsulinemic-euglycemic normal rats³⁶. Further studies are required to ascertain the nature of the disturbance in fat metabolism. Notably, the extent of impairment of fat metabolism is disproportionate to the extent of insulin resistance. For instance, mice with primary hepatic insulin resistance did not develop elevated FFA despite having higher insulin levels than L-SACC1 transgenics^{18,37}. This suggests that impairment of fat metabolism in L-SACC1 mice is related to the mechanism of their insulin resistance (that is, secondary to impaired insulin clearance rather than a primary genetic defect in insulin receptor expression). Altered fat metabolism may explain the persistence of hyperglycemia, glucose intolerance and insulin resistance in L-SACC1 mice as opposed to LIRKO mice that regained hepatic insulin sensitivity at six months of age. The increase in triglyceride content in livers of L-SACC1 transgenics may also suggest that the impairment of fat metabolism is secondary to the change of hepatic insulin sensitivity brought about by the transgene, and not to substrate redistribution as, for instance, in muscle-specific insulin receptor knockouts³⁸. The increase in liver triglycerides may contribute to hepatic insulin resistance that, in turn, may result from hyperinsulinemia. These studies demonstrate a novel mechanism by which

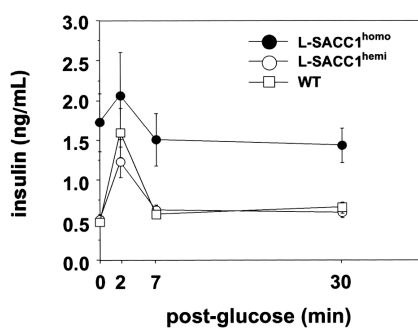


Fig. 6 Normal pancreatic β -cell function in L-SACC1^{homo} mice. We measured insulin secretion in response to glucose injections in 10-mo wildtype (WT, open squares), L-SACC1^{hemi} (open circles) and L-SACC1^{homo} (open squares) mice that had been fasted. Whole blood was drawn at indicated time points from retro-orbital sinuses to determine plasma insulin level. Data represent the average of at least two sets of experiments using a minimum of 12 mice of each genotype. Values are expressed as mean \pm s.e.m..

Table 2 • Elevated levels of free fatty acid and triglycerides in plasma of L-SACC1 mice

Genotype (n)	Plasma free fatty acids (mEq L ⁻¹)		Plasma triglycerides (mg/dL)	
	2 mo	8 mo	2 mo	8 mo
WT (24)	0.356 ± 0.03	0.698 ± 0.03	64.4 ± 7.95	75.37 ± 4.34
L-SACC1 (21)	0.443 ± 0.02*	0.960 ± 0.05*	94.6 ± 9.73*	114.14 ± 8.80*

Fasting plasma FFA and triglycerides were determined in age-matched mice at 2 mo and 8 mo. The number of mice tested is indicated in parentheses. All assays were carried out in triplicate. Values are expressed as mean ± s.e.m. *P<0.05 versus WT mice.

CEACAM1-dependent insulin signaling in hepatocytes is linked to regulation of hepatic insulin sensitivity by modulating insulin metabolism in liver. They also provide *in vivo* evidence of the direct role of insulin clearance in liver in maintaining carbohydrate and fat homeostasis.

Methods

Generation of liver-specific S503A CEACAM1 mice (L-SACC1). We subcloned the 490-bp fragment 5' of the translation start site in genomic DNA of human apolipoprotein A-1 (Apo A-1)^{39,40} upstream of *Ceacam1* cDNA (from S503A rat) into an EcoRI site⁴¹ in pGEM9Z. We introduced intron 1 of rat *Ceacam1* between *Nde*I at nt 10 in exon 1 and *Bam*H I at nt 313 in exon 2 (ref. 41). We re-subcloned the *Not*I-excised Apo A-1/S503A *Ceacam1* minigene in pcDNA3 (Fig. 1a). As seen with ligand-induced receptor internalization, addition of insulin decreased surface expression of biotin-labeled insulin receptor¹⁴ in untransfected SV-40 transformed hepatocytes (UT; Fig. 1b, lanes 2 versus 1). In contrast, in hepatocytes expressing the minigene, internalization of the insulin receptor in the presence of insulin was inhibited (Fig. 1b, lanes 4 versus 3), suggesting that the mutant is dominant-negative. We excised the promoter-minigene-polyadenylation DNA fragment and injected it into the pronuclei of single-cell fertilized mouse embryos derived from C57BL/6 × FVB matings. We identified four F0 founders by Southern blot analysis of genomic DNA from *Hind*III/*Pst*I-digested tail and probing with [³²P]-labeled promoter/S503A *Ceacam1* minigene (Fig. 1c)^{41,42}. Northern blot analysis on poly(A) mRNA (Ambion; data not shown) and western blot analysis using a polyclonal α-CEACAM1 antibody that cross-reacts with rat and mouse proteins indicated that the rat transprotein was detected at high levels in liver of transgenic F1 mice (Fig. 1d) but not in intestines (Fig. 1d) or kidneys (data not shown).

Animal husbandry. We bred hemizygous mice (L-SACC1^{hemi}) to homozygosity by brother/sister matings. We confirmed homozygosity by quantitative Southern blot and empirically by mating homozygous mice (L-SACC1^{homo}). Animals were kept in a 12-h dark-light cycle and fed standard chow *ad libitum*. All procedures described below were approved by the Institutional Animal Care and Utilization Committee.

Phosphorylation. We dissected livers from anesthetized animals and froze them immediately before lysis and partial purification by lectin chromatography⁵. After carrying out insulin-induced phosphorylation in the presence of [γ -³²P]ATP⁵, we immunoprecipitated proteins with anti-biliary glycoprotein (BGP, the mouse homolog of rat CEACAM1) or anti-rat CEACAM1 antibodies and analyzed them using SDS-PAGE and autoradiography. For insulin-receptor and IRS-2 phosphorylation, we carried out the reaction in the absence of [γ -³²P]ATP, immunoprecipitated proteins with monoclonal antibodies against the IR-β subunit or IRS-2, immunoblotted with anti-phosphotyrosine antibodies (α-pTyr) and detected proteins by enhanced chemiluminescence (ECL; Amersham Pharmacia Biotech).

Phenotypic analysis. We measured blood glucose levels using a glucometer (Accu-chek, Boehringer Mannheim), plasma insulin and C-peptides with radioimmunoassays (RIA, Linco), fasting plasma free fatty acids (FFA) using the NEFA C kit (Wako) and triglycerides using the Infinity Triglycerides reagent (Sigma). We determined tissue-triglyceride content in homogenized tissues by extracting lipid with CHCl₃:CH₃OH (2:1, v:v), drying under N₂, resuspending in ethanol, and measuring triglycerides levels as the difference between free and total glycerol⁴³. Liver, muscle and kidney functions were assayed by Analytics.

Metabolic clearance assay. We fasted age-matched 8-mo male mice for 18 h (from 5:00 pm to 12:00 pm the next day) prior to intravenous tail vein injection with 0.05 µg of human recombinant [¹²⁵I]-insulin⁴⁴. We collected venous blood samples (100 µl per mouse) at 7.5, 15, 60 and 90 min after injection, counted 50 ml plasma and measured residual insulin in cpm ml⁻¹ plasma.

Insulin tolerance test. We fasted mice for 19 h (from 4:00 pm to 11:00 am the next day) prior to intraperitoneal injection (i.p.) with insulin (0.125 mU g⁻¹ body weight). We drew venous blood from the retro-orbital sinuses at 0, 30, 60 and 180 min after insulin injection to determine blood glucose levels.

Intraperitoneal glucose tolerance test and insulin secretion. We injected mice fasted overnight with glucose (2 mg kg⁻¹ body weight) i.p. and drew venous blood from the retro-orbital sinuses at 0, 15, 30, 60 and 120 min after injection to determine glucose levels. We simultaneously measured secreted insulin from β-cells in plasma at 2, 7 and 30 min.

Morphometric analysis of pancreas. Pancreata were sectioned into 5-mm³ portions, fixed in 10% formalin-PBS (pH 7.4), ethanol-dehydrated and paraffin-embedded^{37,45}. We mounted consecutive sections on glass slides, rehydrated, permeabilized in 0.1% Triton X-100 and immunostained with mouse insulin antibodies (Sigma). We systematically viewed sections with a Nikon Optiphot-2 microscope (Nikon) and a Spot 1.4.0 video camera (Diagnostic Instruments) with accumulating images from eight non-overlapping fields of 1.5 × 10⁶ mm². We examined at least three sections from three animals per genotype for a total of 18 independent sections. We traced and analyzed β-cells in NIH Image v. 1.60. Data were expressed as percentage of the total area containing insulin-labeled cells.

Primary hepatocytes. We isolated hepatocytes by perfusing with 1 mg ml⁻¹ collagenase in L-15 medium containing 1 mg ml⁻¹ glucose (Gibco BRL). We plated cells at 0.5 × 10⁶ cells per well and incubated at 37 °C in DMEM-FBS-penicillin-streptomycin (Gibco BRL). We refed cultures with DMEM after a 2-h attachment period⁴⁶.

Ligand binding and internalization. We grew primary hepatocytes for 24 h prior to [¹²⁵I]-insulin (10 pM) binding at 4 °C in buffer F (100 mM HEPES, pH 7.4, 120 mM NaCl, 1.2 mM MgSO₄, 1 mM EDTA, 15 mM CH₃COONa, 10 mM glucose, 1% BSA). We removed unbound insulin and incubated cells at 37 °C for 0–90 min before incubating them in 0.1% BSA-PBS (pH 3.5) for 10 min¹¹. We counted the acid wash as surface-bound, non-internalized insulin and NaOH-solubilized cells as internalized cell-associated ligand. We calculated internalized insulin as percent cell-associated per specifically bound ligand (the sum of surface-bound plus cell-associated ligand).

Biotin labeling of surface membrane proteins. After incubation of primary hepatocytes in the absence or presence of 100 nM insulin at 37 °C for 5 min, we incubated cells with biotin as previously described¹⁴. Following lysis in 1% Triton-X, proteins were immunoprecipitated with a monoclonal antibody against BGP (mouse homolog of rat CEACAM1), electrophoresed, immunoblotted with HRP-conjugated streptavidin and detected with ECL.

Insulin-receptor quantification. We incubated primary hepatocytes at 37 °C in triplicate plates for 24 h before incubating at 4 °C for 5 h in Buffer F supplemented with insulin (0, 1, 5, 10, 100 and 1,000 ng ml⁻¹) and [¹²⁵I]-labeled insulin (20 pM; 5.0 × 10⁴ cpm ml⁻¹). NaOH-lysed cells were counted and the IR number determined by Scatchard-plot analysis using the SCAFFIT v. 4.7 program (National Institutes of Health).

Glucose uptake in isolated muscle. As described previously^{47,48}, we removed soleus muscle from hindlimbs of fasted mice^{47,48}, pre-equilibrated it for 1 h in oxygenated Krebs-Henseleit buffer containing 2 mM pyruvate, 36 mM mannitol and 0.1% BSA with or without 1,200 pM insulin, and incubated it at 30 °C at 95% O₂, 5% CO₂ for 20 min in 2-deoxy-D-

[$\text{I},\text{2}^{-3}\text{H}$]glucose (1 mM), [U^{-14}C]mannitol (39 mM) and 0.1% BSA. Muscles were immediately blotted and frozen in liquid nitrogen, and stored at -80°C before digestion, counting and measuring of intracellular 2-DG accumulation in nmol g wet muscle $^{-1}$ min $^{-1}$.

Statistical procedures. We analyzed data with Statview software (Abacus concepts) using one-factor ANOVA analysis. *P* values less than 0.05 were considered to be statistically significant.

Acknowledgments

We thank D. Accili, S.F. Previs and G.I. Shulman for critical reading of the manuscript and for helpful scientific discussions, and E.M. Rubin and N. Beauchemin for providing the apolipoprotein A-1 promoter cDNA and anti-mouse BGP antibodies, respectively. We thank S. Robson, E. Tietz and S. Lilly for assistance in immunohistochemistry and microscopy, and T. Dai and R. Ruch for assistance in primary hepatocytes. We also thank the Ohio University Edison Biotechnology Institute Collaborative Transgenics, Athens, Ohio for performing DNA microinjections as part of their service grant support (to S.M.N.). This work was chiefly supported by two grants from the National Institutes of Health—National Institute of Diabetes & Digestive & Kidney Diseases (to S.M.N.), and partially by Sigma-Tau Research (to S.M.N.) and the Department of Veterans Affairs (to S.K.E.). M.N.P. was partially supported by the Institutional Pre-doctoral National Research Service Award fellowship from the National Institutes of Health.

Competing interests statement

The authors declare that they have no competing financial interests.

Received 30 October; accepted 12 December 2001.

1. Backer, J.M. et al. Insulin stimulation of phosphatidylinositol 3-kinase activity maps to insulin receptor regions required for endogenous substrate phosphorylation. *J. Biol. Chem.* **267**, 1367–1374 (1992).
2. Baumann, C.A. et al. CAP defines a second signalling pathway required for insulin-stimulated glucose transport. *Nature* **407**, 202–207 (2000).
3. Mathews, S.T. et al. Alpha2-HSG, a specific inhibitor of insulin receptor autophosphorylation, interacts with the insulin receptor. *Mol. Cell. Endocrinol.* **164**, 87–98 (2000).
4. Maddux, B.A. & Goldfine, I.D. Membrane glycoprotein PC-1 inhibition of insulin receptor function occurs via direct interaction with the receptor α -subunit. *Diabetes* **49**, 13–19 (2000).
5. Najjar, S.M. et al. Insulin-stimulated phosphorylation of recombinant pp120/HA4, an endogenous substrate of the insulin receptor tyrosine kinase. *Biochemistry* **34**, 9341–9349 (1995).
6. Cheung, P.H. et al. Cell-CAM105 isoforms with different adhesion functions are coexpressed in adult rat tissues and during liver development. *J. Biol. Chem.* **268**, 6139–6146 (1993).
7. Hsieh, J.-T. et al. Tumor suppressive role of an androgen-regulated epithelial cell adhesion molecule (C-CAM) in prostate carcinoma cell revealed by sense and antisense approaches. *Cancer Res.* **55**, 190–197 (1995).
8. Luo, W., Wood, C.G., Earley, K., Hung, M.C. & Lin, S.H. Suppression of tumorigenicity of breast cancer cells by an epithelial cell adhesion molecule (C-CAM1): the adhesion and growth suppression are mediated by different domains. *Oncogene* **14**, 1697–1704 (1997).
9. Rosenberg, M. et al. The expression of mouse biliary glycoprotein, a carcinoembryonic antigen-related gene, is down-regulated in malignant mouse tissues. *Cancer Res.* **53**, 4938–4945 (1993).
10. Neumaier, M., Paululat, S., Chan, A., Matthaeus, P. & Wagener, C. Biliary glycoprotein, a potential human cell adhesion molecule, is down-regulated in colorectal carcinomas. *Proc. Natl. Acad. Sci. USA* **90**, 10744–10748 (1993).
11. Li Calzi, S., Choice, C.V. & Najjar, S.M. Differential effect of pp120 on insulin endocytosis by two variant insulin receptor isoforms. *Am. J. Physiol.* **273**, E801–808 (1997).
12. Formisano, P. et al. Receptor-mediated internalization of insulin. Potential role of pp120/HA4, a substrate of the insulin receptor kinase. *J. Biol. Chem.* **270**, 24073–24077 (1995).
13. Soni, P., Lakkis, M., Poy, M.N., Fernstrom, M.A. & Najjar, S.M. The differential effects of pp120 (Ceacam 1) on the mitogenic action of insulin and insulin-like growth factor 1 are regulated by the nonconserved tyrosine 1316 in the insulin receptor. *Mol. Cell. Biol.* **20**, 3896–3905 (2000).
14. Choice, C.V., Howard, M.J., Poy, M.N., Hankin, M.H. & Najjar, S.M. Insulin stimulates pp120 endocytosis in cells co-expressing insulin receptors. *J. Biol. Chem.* **273**, 22194–22200 (1998).
15. Duckworth, W.C., Bennett, R.G. & Hamel, F.G. Insulin degradation: progress and potential. *Endocr. Rev.* **19**, 608–624 (1998).
16. Han, E. et al. Differences in tissue-specific and embryonic expression of mouse Ceacam1 and Ceacam2 genes. *Biochem. J.* **355**, 417–423 (2001).
17. Chen, X., Iqbal, N. & Boden, G. The effects of free fatty acids on gluconeogenesis and glycogenolysis in normal subjects. *J. Clin. Invest.* **103**, 365–372 (1999).
18. Michael, M.D. et al. Loss of insulin signaling in hepatocytes leads to severe insulin resistance and progressive hepatic dysfunction. *Mol. Cell* **6**, 87–97 (2000).
19. Najjar, S.M., Choice, C.V., Soni, P., Whitman, C.M. & Poy, M.N. Effect of pp120 on receptor-mediated insulin endocytosis is regulated by the juxtamembrane domain of the insulin receptor. *J. Biol. Chem.* **273**, 12923–12928 (1998).
20. Svedberg, J., Stromblad, G., Wirth, A., Smith, U. & Björntorp, P. Fatty acids in the portal vein of the rat regulate hepatic insulin clearance. *J. Clin. Invest.* **88**, 2054–2058 (1991).
21. Escobar, O. et al. Hepatic insulin clearance increases after weight loss in obese children and adolescents. *Am. J. Med. Sci.* **317**, 282–286 (1999).
22. Bosello, O. et al. Modifications of abdominal fat and hepatic insulin clearance during severe caloric restriction. *Ann. Nutr. Metab.* **34**, 359–365 (1990).
23. Peiris, A.N., Mueller, R.A., Smith, G.A., Struve, M.F. & Kisseebah, A.H. Splanchnic insulin metabolism in obesity. Influence of body fat distribution. *J. Clin. Invest.* **78**, 1648–1657 (1986).
24. Svedberg, J., Björntorp, P., Smith, U. & Lonnroth, P. Free-fatty acid inhibition of insulin binding, degradation, and action in isolated rat hepatocytes. *Diabetes* **39**, 570–574 (1990).
25. Hennes, M.M., Shrager, E. & Kisseebah, A.H. Receptor and postreceptor effects of free fatty acids (FFA) on hepatocyte insulin dynamics. *Int. J. Obes.* **14**, 831–841 (1990).
26. Ferrannini, E., Barrett, E.J., Bevilacqua, S. & DeFronzo, R.A. Effect of fatty acids on glucose production and utilization in man. *J. Clin. Invest.* **72**, 1737–1747 (1983).
27. Kisseebah, A.H., Alfarsi, S., Adams, P.W. & Wynn, V. Role of insulin resistance in adipose tissue and liver in the pathogenesis of endogenous hypertriglyceridaemia in man. *Diabetologia* **12**, 563–571 (1976).
28. Rooney, D.P. & Robertson, R.P. Hepatic insulin resistance after pancreas transplantation in type I diabetes. *Diabetes* **45**, 134–138 (1996).
29. Diem, P., Abid, M., Redmon, J.B., Sutherland, D.E. & Robertson, R.P. Systemic venous drainage of pancreas allografts as independent cause of hyperinsulinemia in type I diabetic recipients. *Diabetes* **39**, 534–540 (1990).
30. Bergman, R.N. & Ader, M. Free fatty acids and pathogenesis of type 2 diabetes mellitus. *Trends Endocrinol. Metab.* **11**, 351–356 (2000).
31. Bergman, R.N. Non-esterified fatty acids and the liver: why is insulin secreted into the portal vein? *Diabetologia* **43**, 946–952 (2000).
32. Reaven, G.M. & Chen, Y.D. Role of insulin in regulation of lipoprotein metabolism in diabetes. *Diabetes Metab. Rev.* **4**, 639–652 (1988).
33. Randle, P.J., Garland, P.B., Newsholme, E.A. & Hales, C.N. The glucose fatty acid cycle in obesity and maturity onset diabetes mellitus. *Ann. NY Acad. Sci.* **131**, 324–333 (1965).
34. Randle, P.J., Priestman, D.A., Mistry, S. & Halsall, A. Mechanisms modifying glucose oxidation in diabetes mellitus. *Diabetologia* **37**, S155–161 (1994).
35. Nestel, P.J., Ishikawa, T. & Goldrick, R.B. Diminished plasma free fatty acid clearance in obese subjects. *Metabolism* **27**, 589–597 (1978).
36. Koopmans, S.J., Kushwaha, R.S. & DeFronzo, R.A. Chronic physiologic hyperinsulinemia impairs suppression of plasma free fatty acids and increases *de novo* lipogenesis but does not cause dyslipidemia in conscious normal rats. *Metabolism* **48**, 330–337 (1999).
37. Kido, Y. et al. Tissue-specific insulin resistance in mice with combined mutations in the insulin receptor, IRS-1, and IRS-2. *J. Clin. Invest.* **105**, 199–205 (2000).
38. Kim, J.K. et al. Redistribution of substrates to adipose tissue promotes obesity in mice with selective insulin resistance in muscle. *J. Clin. Invest.* **105**, 1791–1797 (2000).
39. Walsh, A., Ito, Y. & Breslow, J.L. High levels of human apolipoprotein A-I in transgenic mice result in increased plasma levels of small high density lipoprotein (HDL) particles comparable to human HDL. *J. Biol. Chem.* **264**, 6488–6494 (1989).
40. Bisaha, J.G., Simon, T.C., Gordon, J.I. & Breslow, J.L. Characterization of an enhancer element in the human apolipoprotein C-III gene that regulates human apolipoprotein A-I gene expression in the intestinal epithelium. *J. Biol. Chem.* **270**, 19979–19988 (1995).
41. Najjar, S.M. et al. pp120/ecto-ATPase, an endogenous substrate of the insulin receptor tyrosine kinase, is expressed as two variably spliced isoforms. *J. Biol. Chem.* **268**, 1201–1206 (1993).
42. Najjar, S.M. et al. Cloning and characterization of a functional promoter of the rat pp120 gene, encoding a substrate of the insulin receptor tyrosine kinase. *J. Biol. Chem.* **271**, 8809–8817 (1996).
43. Folch, J., Lees, M. & Sloane-Stanley, G.H. A simple method for the isolation and purification of total lipids from animal tissues. *J. Biol. Chem.* **226**, 497–509 (1957).
44. Mondon, C.E., Olefsky, J.M., Doklas, C.B. & Reaven, G.M. Removal of insulin by perfused rat liver: effect of concentration. *Metabolism* **24**, 153–160 (1975).
45. Cinti, S., Eberbach, S., Castellucci, M. & Accili, D. Lack of insulin receptors affects the formation of white adipose tissue in mice. A morphological and ultrastructural analysis. *Diabetologia* **41**, 171–177 (1998).
46. Ruch, R.J. & Klaunig, J.E. Kinetics of phenobarbital inhibition of intercellular communication in mouse hepatocytes. *Cancer Res.* **48**, 2519–2523 (1988).
47. Lee, A.D., Gulve, E.A., Chen, M., Schluter, J. & Holloszy, J.O. Effects of Ca^{2+} ionophore ionomycin on insulin-stimulated and basal glucose transport in muscle. *Am. J. Physiol.* **268**, R997–1002 (1995).
48. Lee, C.H. et al. Nck associates with the SH2 domain-docking protein IRS-1 in insulin-stimulated cells. *Proc. Natl. Acad. Sci. USA* **90**, 11713–11717 (1993).